LIMNOLOGY and OCEANOGRAPHY LETTERS

ASLO

Open Access

Limnology and Oceanography Letters 2025

doi: 10.1002/lol2.70043

LETTER

High Antarctic coastal productivity in polynyas revealed by considering remote sensing ice-adjacency effects

Hilde Oliver [1]* **Jessica S. Turner** [2] **Alexandre Castagna** [3] **Henry Houskeeper** [1] **Heidi Dierssen** [4]

[1]Woods Hole Oceanographic Institution, Woods Hole, Massachusetts, USA; [2]Department of Ocean and Earth Sciences, Old Dominion University, Norfolk, VA, USA; [3]Ghent University, Ghent, Belgium; [4]University of Connecticut, Groton, Connecticut, USA

Scientific Significance Statement

Satellite-based estimates of Antarctic coastal primary productivity are underpinned by ocean-color algorithms of chlorophyll *a* (Chl *a*), which indicate highest concentrations away from the icy coast. However, ocean color retrievals of Chl *a* in water can be severely impacted by atmospheric scattering of light reflecting off nearby floating ice and snow-covered land (termed adjacency effect). Using satellite estimates, in situ measurements, and modeling, this study explores how adjacency effects impact retrievals of Antarctic coastal Chl *a* and subsequent estimation of net primary productivity (NPP). We find that satellite-based estimates of net primary production more than double in over half of Antarctic coastal polynyas when satellite imagery is processed using approaches that mitigate adjacency effects. Presently, such approaches have generally not been applied in analyses of Antarctic coastal productivity trends. Our findings suggest that Antarctic primary productivity is likely to be substantially higher near the icy coastlines than has been estimated from using remote sensing with standard processing, in which atmospheric correction is highly sensitive to ice adjacency.

Abstract

Ocean color-based estimates of Antarctic net primary productivity (NPP) have indicated low nearshore productivity in ice-adjacent waters, contrasting with coupled physical–biogeochemical models. To understand this discrepancy, we assessed satellite records of polynya NPP by comparing field data with two satellite imagery datasets derived using different processing schemes. Our results indicate historical underestimation of chlorophyll *a* for imagery obtained using default atmospheric correction processing within approximately 100 km of ice-covered coastlines due to adjacency effects. Using radiative transfer modeling, we find that biases in ocean color polynya observations due to adjacency effects correspond to the high albedo of ice and snow. When applying an atmospheric correction processing scheme more robust to adjacency contamination, estimates of NPP more than doubled in 65% of polynyas, especially smaller eastern Antarctic polynyas. Adjacency effects should therefore be accounted for when analyzing spatial and temporal trends in Antarctic coastal primary productivity.

*Correspondence: holiver@whoi.edu

Associate editor: Raphael Kudela

Data Availability Statement: All derived and modeled 10-yr climatologies (OBPG/L2gen Chl *a*, OBPG/L2gen nFLH, OC-CCI Chl *a*, OBPG/L2gen modeled VGPM NPP, and OC-CCI modeled VGPM NPP) and satellite/in situ data matchups are archived at Zenodo at https://doi.org/10.5281/zenodo.15231504.

Embedded within sea ice on the Antarctic continental shelf, Antarctic coastal polynyas are considered to be hotspots of Southern Ocean primary productivity associated with high concentrations of chlorophyll a (Chl *a*) (Arrigo et al. 2015, 2008a). Remote sensing algorithms for Antarctic coastal net primary productivity (NPP) are largely underpinned by ocean color-based estimates of Chl *a* (Arrigo et al. 2008b, 2015; Dierssen et al. 2000). Surface Chl *a* alone can explain over 60% of the variability in Antarctic coastal NPP, lending itself to use in productivity models (Dierssen et al. 2000), but estimating Antarctic coastal Chl *a* from ocean color is not straightforward. Traditional satellite Chl *a* algorithms may underestimate Antarctic coastal Chl *a* due to the region's unique inherent optical properties (Dierssen and Smith 2000; Reynolds et al. 2015; Zeng et al. 2016).

Large errors in satellite-derived Chl *a* at moderate-to-high concentrations are known to occur near sea ice due to adjacency effects using standard atmospheric corrections (Bélanger et al. 2007). The adjacency effect is the blurring of surface reflectance patterns due to atmospheric scattering, both downwards (spherical albedo) and upwards (diffuse upward transmittance). The higher the contrast in surface reflectance and atmospheric scattering, the higher the blurring effect. Ice and snow-covered land surrounding water is an example of extreme surface contrast found in polynyas. Light reflected from the relatively bright surfaces will be scattered by the atmosphere into the field of view of the sensor when looking over the relatively dark water surfaces. This adjacency signal must be compensated for when retrieving surface reflectances from top-of-atmosphere observations, or can result in significant overestimation of reflectance and distortion of the reflectance spectral shape (Bulgarelli et al. 2014; Tanre et al. 1979, 1981). In the Canadian Arctic, adjacency effects and subpixel floating ice render Chl *a* estimates within ~ 10–20 km of the sea ice edge unreliable (Bélanger et al. 2007).

Previous estimates of Antarctic coastal NPP have assessed satellite Chl *a* products derived using the standard NASA Ocean Biology Processing Group (OBPG) atmospheric correction. The atmospheric correction method used by OBPG is based on the assumption of zero near-infrared water reflectance to estimate aerosol properties (aka "black pixel" approach), with an iterative step to compensate for possible non-zero near-infrared reflectance (Bailey et al. 2010). It will be termed here as "OBPG/L2gen," as the method is implemented in the L2gen module of the SeaDAS software (Mobley et al. 2016). Chl *a* is estimated from the retrieved water reflectance using a blending algorithm for low and high Chl *a* concentrations (Hu et al. 2019). The OBPG/L2gen method is applied pixel per pixel and does not account for adjacency effects.

In contrast, the Chl *a* product provided by the European Space Agency Climate Change Initiative (CCI) Ocean Color project (OC-CCI) instead applies the atmospheric correction known as "Polynomial-Based Algorithm Applied to MERIS" (POLYMER). This method uses iterative spectral matching to separate contributions for atmosphere and interface (glint) from that of water, where the water component is based on a bio-optical model and the nonwater components are treated, in polynomial form, as a function of wavelength. Chl *a* is then estimated from the retrieved water reflectance by blending optical water type specific methods (Jackson et al. 2017). While POLYMER is also applied pixel per pixel and does not account for adjacency explicitly, its zeroth order (i.e., spectrally flat) polynomial term can mitigate adjacency from snow, ice, and clouds due to their similar spectral shape in the visible to near-infrared range. Therefore, POLYMER has the potential to better account for adjacency effects arising from ice and snow and demonstrates improved performance in Arctic and coastal waters (Frouin et al. 2012; IOCCG 2015; König et al. 2019, 2; Soppa et al. 2021). Nonetheless, standard atmospheric corrected Level 2 or Level 3 products have been used in past assessments of NPP in Antarctic polynyas, which may have been impacted by adjacency effects (Arrigo et al. 2015; Yager et al. 2012).

This study complements previous work on adjacency in the Arctic (Bélanger et al. 2007; Frouin et al. 2012; IOCCG 2015) by evaluating adjacency effects as observed by the Moderate Resolution Imaging Spectroradiometer (MODIS) onboard the Aqua satellite (MODIS/Aqua) sensor over the glaciated coastal Antarctic. We investigate the bias caused by adjacency by comparing imagery from different atmospheric correction algorithms (POLYMER and OBPG/L2gen) to field data and evaluating Chl *a* from POLYMER and OBPG/L2gen relative to their distance from the icy coastline. We corroborate our findings using radiative transfer simulations to demonstrate expected impacts of adjacency on OBPG/L2gen Chl *a* products. With these results we consider how adjacency effects may impact NPP estimates on the Antarctic continental shelf.

Methods

Chl *a* product comparisons

We compared 4-km resolution Chl *a* products from MODIS/Aqua, available from OBPG/NASA (reprocessing R2022.0), and the multisensor merged product available from European Space Agency OC-CCI v6.0. Our analysis focused on a decadal average (2010–2019) for January, the month that experiences peak annual NPP in Antarctic coastal polynyas (Arrigo et al. 2015). The decadal average provides a more spatially complete dataset and accounts for interannual variability. The comparison was made for the Antarctic shelf, defined inshore of the 1500 m isobath. The MODIS/Aqua product uses OBPG/L2gen atmospheric correction, while the OC-CCI v6.0 merged product uses POLYMER atmospheric correction

(OC-CCI 2022). The OC-CCI v6.0 merged product is generated by band-shifting and bias-correcting data from SeaWIFS (1997–2010), MODIS-Aqua (2002–2019), SNPP-VIIRS (2012–2019), S3A-OLCI (2016 to ongoing), and S3B-OLCI (2018 to ongoing) to match MERIS (2002–2012). The OBPG/L2gen algorithm is an iterative two-band bio-optical–based algorithm, initially implemented during the SeaWiFS era (Gordon and Wang 1994), which now includes the more recent Multi Band Atmospheric Correction processing developed for PACE (Ibrahim et al. 2019). POLYMER is a spectral matching-based algorithm (Steinmetz et al. 2011).

We implemented a 4th-order polynomial following Dierssen and Smith (2000) to improve the regional accuracy of our Chl *a* estimation as standard NASA Chl *a* retrievals tend to underestimate Chl *a* in Antarctic coastal waters, particularly at higher concentrations (Dierssen et al. 2000; Ferreira et al. 2022). The reasons for this underestimation at Chl *a* values > 0.5 mg m^{-3}, are still being investigated and can result from both increased blue reflectance and decreased green reflectance as Chl *a* increases. Such underestimation may result from lower phytoplankton absorption per Chl *a* (higher pigment "packaging"), as well as lower amounts of CDOM and lower particulate backscattering that may be coupled to chlorophyll in a non-standard manner (i.e., Case 1 waters). We also evaluated the MODIS/Aqua normalized fluorescence line height (nFLH; Letelier and Abbott 1996) obtained for MODIS/Aqua imagery using the OBPG/L2gen processing. Normalized fluorescence line height is expected to be less sensitive to adjacency effects from ice and snow because it is capturing Chl *a* fluorescence signal and because it is derived using a difference (e.g., rather than a band-ratio) algorithm applied to two spectrally adjacent wavebands.

To compare satellite Chl *a* to in situ Chl *a*, we used field data from multiple coastal environments in western Antarctica (Supporting Information Table S1). We compiled west Antarctic in situ Chl *a* measurements from three regions: (1) the West Antarctic Peninsula (WAP) (PALmer LTER; Palmer Station Antarctica LTER and Waite 2022); (2) the Amundsen Sea (Amundsen Sea Polynya International Research Expedition) (Arrigo 2015; Yager et al. 2012) and Korea Polar Research Institute cruises for 2014 (Yang 2023), 2016 (Lee 2023a), 2018 (Lee 2023b), and 2020 (Lee 2023c); and (3) the Ross Sea (Smith and Kaufman 2018). Matchups used the closest geographic pixel, with $\pm$ 24-h time window criteria. Matchups used MODIS and OC-CCI datasets for satellite Chl *a* values and compared the results. We only used MODIS data until 2019, given concerns of reduced data quality due to aging sensors. The OC-CCI product containing POLYMER-corrected data covers the period from 2002 to the present, and its merging of multiple sensors results in more opportunities for matchups (1333 vs. 929 matchups with MODIS). Only in situ observations with Chl *a* concentrations greater than 0.05 mg m^{-3} were used.

Net primary productivity calculations

To evaluate how different atmospheric corrections may impact estimates of NPP, we ran a vertically generalized productivity model (VGPM) optimized for Antarctic coastal waters (Dierssen et al. 2000) using the decadal-average Chl *a* product from OBPG/L2gen and OC-CCI, supplemented with sea-surface temperature and photosynthetically available radiation observations obtained from OBPG/L2gen. Where photosynthetically available radiation is missing, we apply a surface photosynthetically available radiation of 40 W m^{-2}, the approximate mean January coastal photosynthetically available radiation level as calculated for the period.

Radiative transfer simulations

To independently assess potential impacts of adjacency to near-ice Chl *a* retrieval, we simulate uncorrected adjacency effects on the MODIS/Aqua OBPG/L2gen Chl *a* algorithm using radiative transfer modeling. For these simulations we calculate the spatially resolved spherical albedo function and the total atmospheric point spread function to propagate the surface reflectance to the top of atmosphere (Castagna and Vanhellemont 2025). The surface reflectance is then calculated from the simulated top-of-atmosphere signal, without accounting for adjacency.

Similarly to Bélanger et al. (2007), we consider two adjacent semi-infinite surfaces representing water and snow-covered ice (Supporting Information Fig. S1a). We apply median water reflectance spectra observed by Dierssen and Smith (2000) for five different Chl *a* concentrations (0.1, 0.5, 1, 5 and 10 mg m^{-3}) in Antarctic waters for the water surface (Supporting Information Fig. S1b), and apply a reflectance for the ice/snow surface from Warren (2013) for optically thick snow. We simulate the atmosphere properties using standard surface pressure and maritime aerosol models with aerosol optical thickness at 550 nm equal to 0.04 at three different observation zenith angles: 0°, 27°, and 55° (Supporting Information Fig. S1c). Due to the asymmetry of the atmospheric point spread function for slanted observations, we perform the simulations for both the left and right side of the observation swath. We then correct the simulated image at the top of atmosphere with perfect information of the atmosphere's composition, which allows us to evaluate how the uncorrected signal arising from adjacency propagates through the OCI Chl *a* algorithm. Further details on the radiative transfer modeling methods are provided in Appendix B in the Supporting Information.

Results

Adjacency effects on coastal Chl *a* estimates

On the west Antarctic shelf, in a domain extending from the Ross Sea to the WAP, different Chl *a* products revealed substantially different spatial patterns, particularly near the coast (Fig. 1). While MODIS/Aqua Chl *a* concentrations

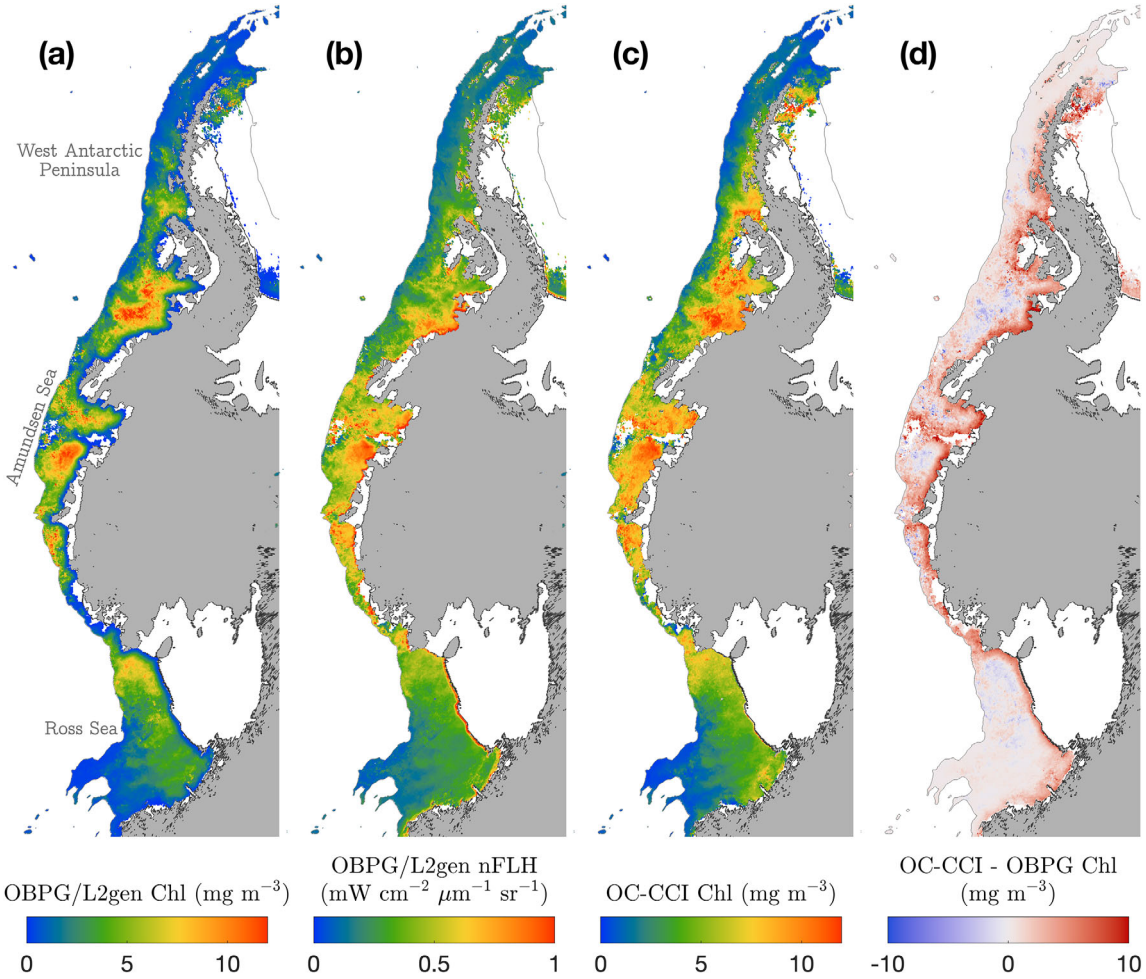

Fig. 1. January 10-yr (2010–2019) mean (**a**) OBPG/L2gen Chl *a*, (**b**) OBPG nFLH, (**c**) OC-CCI Chl *a*, and (**d**) difference in Chl *a* products OC-CCI Chl *a* minus OBPG/L2gen Chl *a*, over the west Antarctic shelf.

decreased near the Antarctic coastline (Fig. 1a), OC-CCI coastal Chl *a* concentrations remained elevated near the ice edges and coastlines, driving a consistent positive Chl *a* anomaly (anomaly defined as the difference between OC-CCI and MODIS) extending along the coast (Fig. 1d). Positive OC-CCI Chl *a* anomalies were also present further from the coast in Amundsen Sea in the eastern Amundsen Sea Polynya and western Pine Island Polynya, approximately where the icebergs comprising Thwaites Iceberg Tongue are grounded. Patterns in OC-CCI Chl *a* (Fig. 1c) were more closely related to the MODIS nFLH (Fig. 1b) (Spearman's rank correlation coefficient $\rho = 0.75$), consistent with nFLH being a normalized difference index less susceptible to atmospheric correction issues and adjacency from ice/snow.

When considering the Chl *a* differences as a function of distance from the shore, the median percentage difference in OC-CCI Chl *a* relative to OBPG/L2gen Chl *a* reached 600% (Interquartile range, IQR: 257–1117%) at the coastline (Fig. 2a). The percentage difference in Chl *a* decreased exponentially with increasing distance from the coast: OC-CCI Chl *a* was reduced to 82% (IQR: 38–165%) that of MODIS at 40 km, and was roughly the same at ~100 km.

To assess the performance of the two different remote sensing products in capturing coastal Chl *a* variability, we compared satellite matchups (with satellite retrievals of Chl *a* regionally tuned using the 4th-order polynomial from Dierssen and Smith (2000)) with the compilation of in situ surface Chl *a* measurements within and beyond 100 km of the coastline (Fig. 3). For measurements made further than 100 km from the coast, both OC-CCI and OBPG/L2gen products captured similar spatial patterns and variability in measured Chl *a* concentrations, with Spearman's $\rho = 0.89$ and $\rho = 0.86$, respectively. (Fig. 3a,b). The Dierssen and Smith (2000) correction on the Chl *a* introduced a positive mean bias, though there was a nearly equivalent negative mean bias for both products without the correction applied (Supporting Information Fig. S2). Within 100 km of the coast, however, the performance of both products was degraded, though

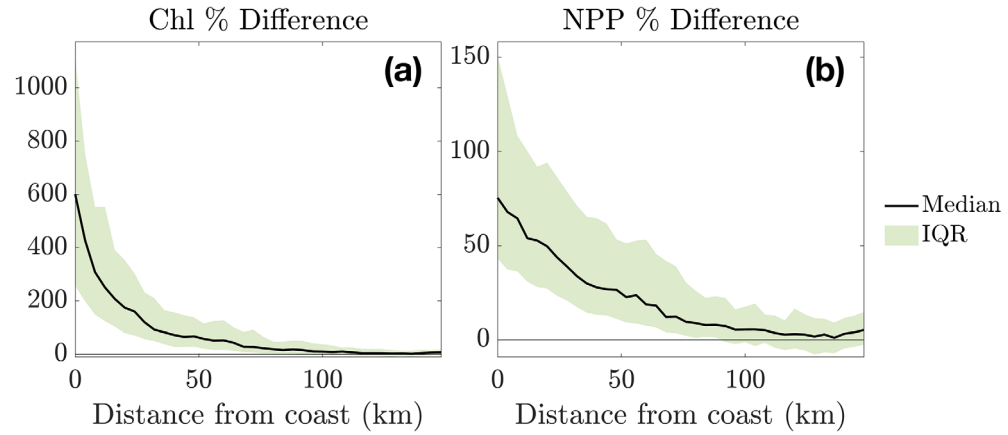

Fig. 2. Percentage difference in OC-CCI and OBPG/L2gen (**a**) Chl *a* and (**b**) modeled VGPM NPP vs. distance from the coast, in 4-km bins, for January 10-yr average products (2010–2019).

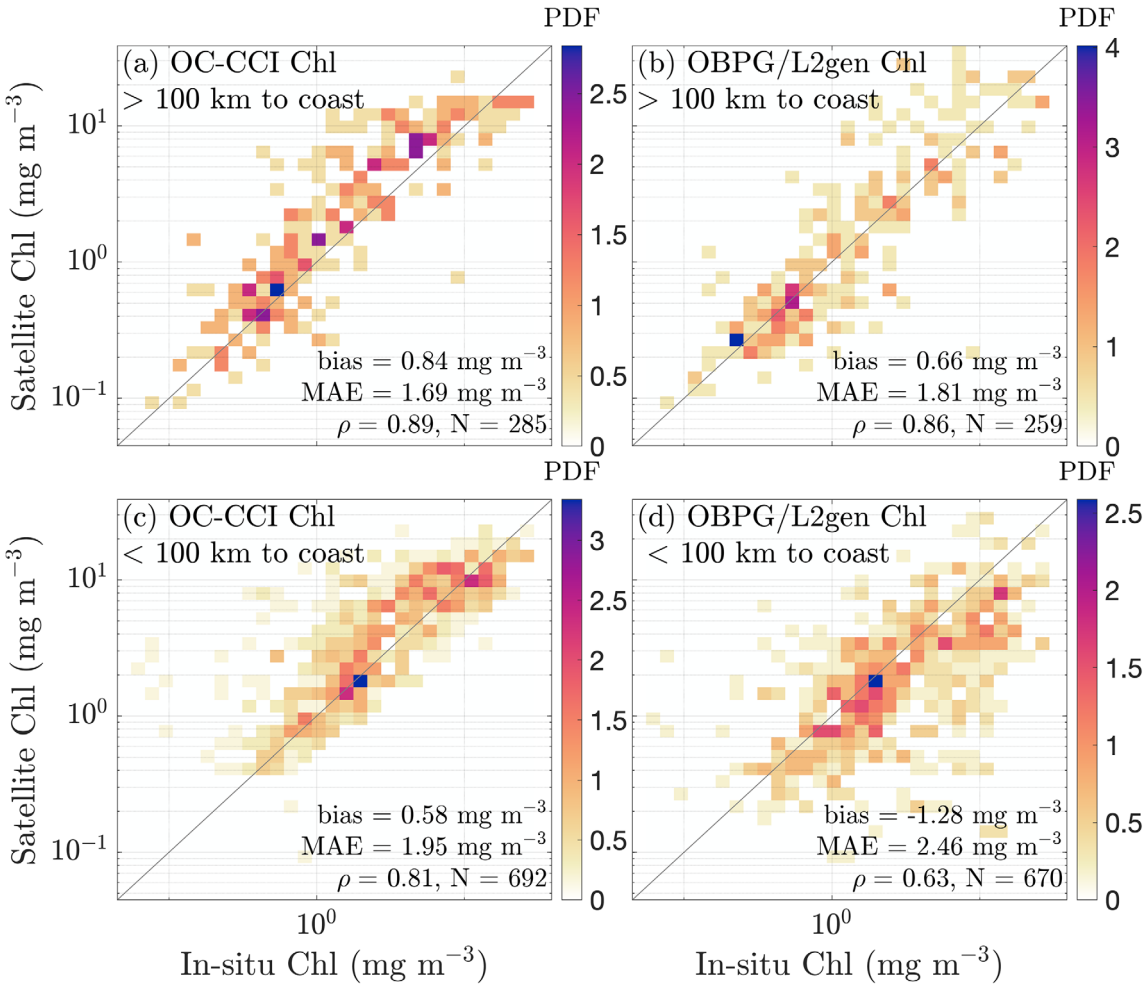

Fig. 3. Satellite chlorophyll (corrected with Dierssen and Smith, 2000) vs. in situ chlorophyll binned scatterplots for OC-CCI (left), OBPG/L2gen (right), further than 100 km from the coast (top), and within 100 km of the coast (bottom). Black lines show 1–1. Mean bias, mean absolute error (MAE), and Spearman's ρ coefficients and number of matchups are included on each subplot. Supporting Information Fig. S2 shows the same data without the Dierssen and Smith (2000) correction applied.

OC-CCI shows improved performance relative to OBPG/L2gen ($\rho = 0.81$ vs $\rho = 0.63$, respectively) (Fig. 3c,d).

Simulating the impact of uncorrected adjacency effects on the retrieval of Chl *a* with the OBPG/L2gen blending algorithm also suggests large impacts on coastal Chl *a* within 100 km of the coast (Fig. 4). The simulated fractional point spread function over ice and snow indicates the degree of mixing between the water diffuse reflectance spectrum and the ice/snow spectrum, as a function of distance from the coast (Fig. 4A). The magnitude of adjacency effects over water is sensitive to the view zenith angle: The greatest adjacency effect was calculated for a −55° view zenith angle (where the sensor is over the ice/snow and looking toward the water, Supporting Information Fig. S1), lesser impacts for −27° and +55°, and the smallest impacts for nadir observations and +27° view zenith angle. Regardless of observation geometry, however, simulated Chl *a* concentrations were sharply reduced relative to their in situ concentration within ~50 km of the coastline, reaching a minimum at the ice-ocean interface (Fig. 4b–f). Note that Chl *a* was still underestimated beyond the distance where it is subject to adjacency effects, as the OBPG/L2gen Chl *a* algorithm underestimates Chl *a* in Western Antarctic coastal waters (Dierssen and Smith 2000).

Polynya NPP

Using POLYMER/OC-CCI Chl *a* in place of OBPG/L2gen Chl *a* yielded substantially greater NPP estimates, especially near the coast and in smaller polynyas (Table 1; Fig. 2). When applying a VGPM model with the different Chl *a* products, polynya NPP was 75% greater (median for 46 polynyas) using OC-CCI Chl *a* (IQR 43–151%) (Fig. 2b). Like Chl *a*, the difference in NPP also decreased with increasing distance from shore, with differences dropping to < 10% at ~ 80 km from shore.

To estimate how adjacency may affect polynya productivity estimates, we then calculated the 10-yr average NPP over each of the 46 polynya masks identified in Arrigo et al. (2015) (map in Supporting Information Fig. S3), using OBPG/L2gen and OC-CCI Chl *a* products corrected with Dierssen and Smith (2000) and compared the magnitude of the changes in NPP estimates between products (Table 1). Across all polynyas, NPP increased by 23% when using OC-CCI Chl *a*. Net primary productivity increased the least (17%) in the largest polynya, the Ross Ice Shelf polynya, and most (353%) in the East Lazarev Ice Shelf polynya, a small east Antarctic polynya. Net primary productivity more than doubled in 65% of polynyas, with the largest effect concentrated in the smaller East Antarctic polynyas in the Weddell Sea and Dronning Maud Land region and the Indian Sector. Polynya size explained most of the variability in the NPP percentage increase ($R^2 = 0.66$, Fig. 5). While remaining generally less productive than western Antarctic polynyas, East Antarctic polynyas saw a marked increase from generally low productivity with OBPG/L2gen (0.79 ± 0.44 g m^{-2} d^{-1}) to a much more productive 1.89 ± 0.57 g m^{-2} d^{-1}. While the Amundsen Sea Polynya has generally been considered the most intensely productive polynya per unit area (Arrigo et al. 2012), with OC-CCI Chl *a*, Eltanin Bay, a polynya in the western Bellingshausen Sea, showed the highest productivity. In general, many of the smaller polynyas increased in NPP rank with OC-CCI processing, with approximately 67% of the polynyas smaller than 10,000 km^2 increasing rank. (Table 1).

Discussion

Our analysis suggests that coastal Chl *a* concentrations and NPP near Antarctic icy coasts are likely to be substantially higher than most previous satellite-based estimates applying the OBPG/L2gen atmospheric correction, owing to adjacency effects. Our analyses considered OBPG/L2gen because it is widely used, but similar degradations in Chl *a* retrievals would be anticipated for other atmospheric processing schemes with high sensitivity to adjacency. The decrease in Chl *a* due to adjacency is not distributed homogenously across polynyas; adjacency effects on polynya NPP estimates are highly related to polynya size (Fig. 5) and thus alter comparisons of the relative differences between polynyas (Table 1). When applying an atmospheric correction less susceptible to adjacency effects arising from snow (POLYMER), there is a multifold increase in Chl *a* concentrations at the coast relative to the OBPG/L2gen atmospheric correction (median > 600% increase, Fig. 2). Comparisons of Chl *a* concentrations produced using different atmospheric correction algorithms (Fig. 2) and simulations (Fig. 4) both independently indicate that the adjacency effects most deleteriously alter Chl *a* retrivals within approximately 50 km of the icy coastline, though biases were observed to extend to at least 100 km from the coast. The similarity between OC-CCI Chl *a* product and the OBPG/L2gen nFLH also suggests that differences are mainly caused by adjacency effects. Normalized fluorescence line height is expected to be less sensitive to additive flat offsets caused by adjacency from ice/snow. Our results also suggest that adjacency effects extend farther offshore than previously thought in high latitude regions, as well as any water body experiencing partial or fully iced conditions or near snow-covered surrounding land surfaces in winter. In this study, these biases extend farther from the coast (50–100 km) than the distances other studies have described for adjacency effects (e.g., 10–20 km in Bélanger et al. 2007; a discussion of the large increase in modeled adjacency is provided in Appendix C in the Supporting Information).

Adjacency effects appear to be most severe along the coast and in small polynyas, which are preferred by emperor penguins for foraging over larger, persistent polynyas (Labrousse et al. 2019). Past remotely sensed NPP estimates suggested low productivity near the Antarctic coastline, while coupled physical–biogeochemical modeling suggested elevated productivity occurring in the Antarctic Coastal Current near the icy

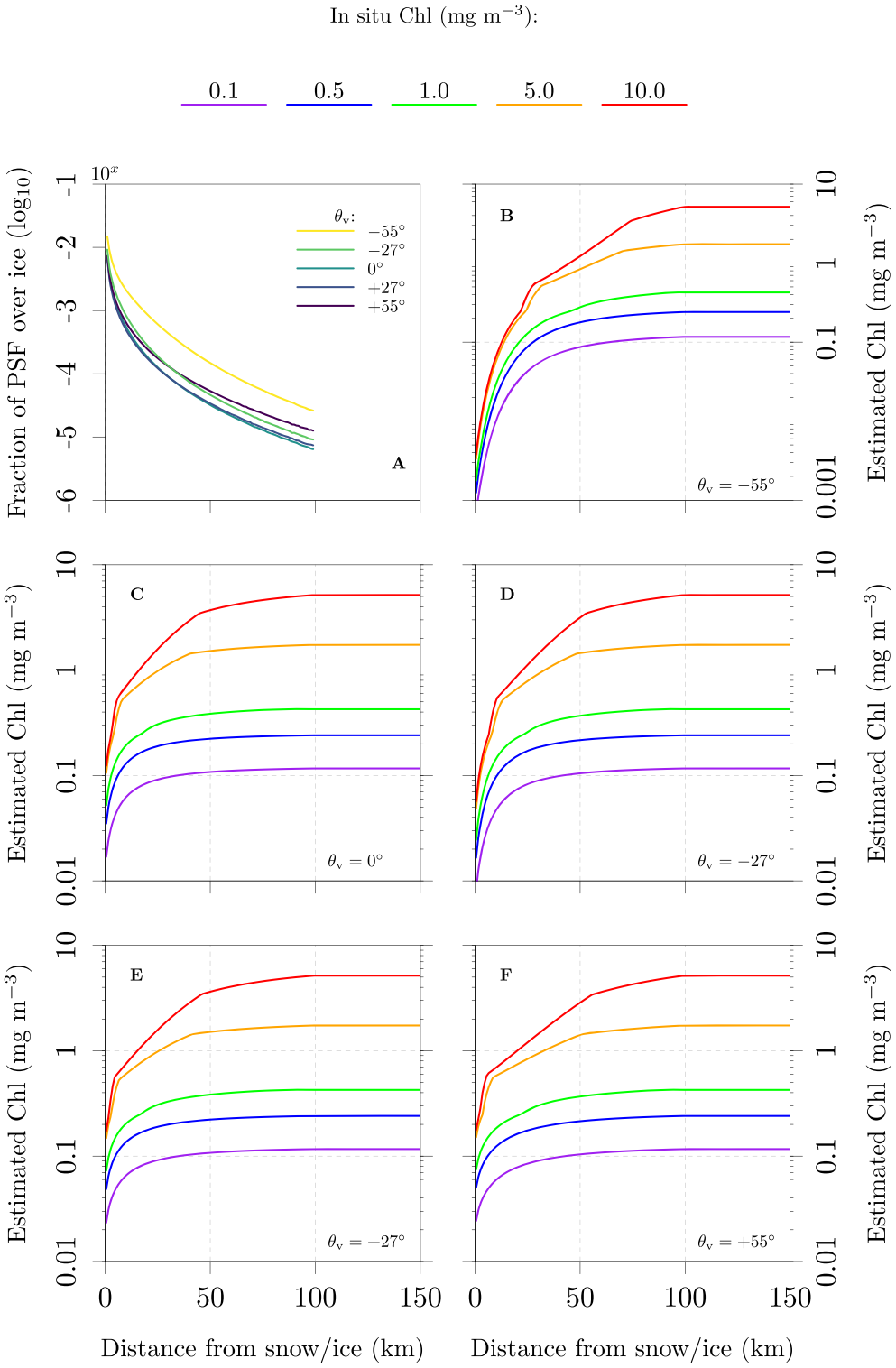

Fig. 4. Effect of uncorrected adjacency effects in MODIS/Aqua OBPG Chl retrieval algorithm. (**a**) The fraction of the total upward transmittance that occurs over snow or ice as a function of distance from snow or ice for different observation geometries. (**b**–**f**) The underestimation of Chl *a* intrinsic to the OBPG algorithm in Antarctic waters and the additional underestimation caused by adjacency as a function of distance from snow-covered ice. The radius of the spatial kernels f_{saf} and f_{psf} was 100 km.

Table 1. Statistics for the 46 Polynyas identified in Arrigo et al. (2015), including the Arrigo et al. (2015) reported mean polynya open water area for 1998–2014, polynya January mean NPP for different Chl *a* products 2010–2019, the change in rank using OC-CCI, and the percentage change in NPP when using OC-CCI Chl, with polynyas where NPP more than doubled shown in bold. Polynyas are sorted from west to east, starting just west of the Ross Ice Shelf. A map of polynya masks is provided in Supporting Information Fig. S3.

ID	Polynya name	SOOS region	Mean open water area (10^3 km^2)	OBPG/L2gen NPP (g m^{-2} d^{-1})	OC-CCI NPP (g m^{-2} d^{-1})	Rank change	NPP % increase
1	Sulzberger Bay	Ross Sea	6.5	1.4	3	14 → 9	**115**
2	Hull Bay	Amundsen/ Bellingshausen Sector	6.4	1.8	3.5	9 → 5	96
3	Wrigley Gulf		11.1	2	3.6	4 → 4	80
4	Amundsen Sea		31.8	3	4	1 → 2	33
5	Pine Island Bay		19.7	2.3	3.8	2 → 3	62
6	Eltanin Bay		11.3	1.9	4.1	6 → 1	**113**
7	Ronne Entrance		15.1	2	3.4	5 → 6	73
8	Marguerite Bay	West Antarctic Peninsula	4.3	1.6	3.1	10 → 8	95
9	Larsen Ice Shelf	Weddell Sea and Dronning Maud Land	4.7	0.6	2.6	32 → 13	**324**
10	Ronne Ice Shelf		44.7	0.9	2.1	23 → 23	**134**
11	Brunt Ice Shelf		15.2	1.3	2.5	18 → 15	**101**
12	Lyddan Island		6	0.9	2.6	22 → 14	**180**
13	Seal Bay		4.3	0.7	1.9	29 → 26	**191**
14	Cape Norvegia		2.3	0.6	1.8	33 → 34	**195**
15	Jelbart Ice Shelf		2.2	0.8	1.8	25 → 31	**140**
16	Fimbul Ice Shelf		3.5	0.6	1.8	31 → 30	**182**
17	W. Lazarev Ice Shelf		1	0.6	1.6	30 → 37	**152**
18	E. Lazarev Ice Shelf		2	0.4	1.9	41 → 28	**353**
19	Breid Bay		1.1	0.6	2.4	34 → 17	**305**
20	Vestvika Bay		2.4	0.8	2.4	24 → 18	**209**
21	Lutzoh-Holm Bay	Indian Sector	1.7	0.1	0.3	46 → 46	**284**
22	Amundsen Bay		1.8	0.4	1.2	39 → 43	**185**
23	Cape Borle		4.3	0.4	1	38 → 45	**122**
24	Stefansson Bay		2.1	1	1.8	21 → 33	83
25	Holme Bay		4.7	1.3	2.1	17 → 25	57
26	Bjerkø Peninsula		12.1	1.4	2.2	13 → 20	54
27	MacKenzie Bay		1.9	1	3.2	19 → 7	**211**
28	Prydz Bay		54.5	1.8	2.5	7 → 16	37
29	West Ice Shelf		2.1	0.4	1.3	42 → 41	**221**
30	Farr Bay		26.7	1.4	2.2	16 → 19	62
31	Mill Island		2.5	0.7	1.9	26 → 27	**161**
32	Cape Nutt		1.5	0.4	1.8	40 → 32	**327**

(Continues)

Table 1. Continued

ID	Polynya name	SOOS region	Mean open water area (10^3 km^2)	OBPG/L2gen NPP (g m^{-2} d^{-1})	OC-CCI NPP (g m^{-2} d^{-1})	Rank change	NPP % increase
33	Vincennes Bay		12.3	1	2.1	20 → 24	**110**
34	Cape Poinsett		4	0.5	1.6	36 → 39	**196**
35	Totten Glacier		1.4	0.5	1.9	37 → 29	**281**
36	Henry Bay		6.5	0.7	1.7	28 → 35	**154**
37	Paulding Bay		1.6	0.4	1.4	44 → 40	**264**
38	Porpoise Bay		1.7	0.4	1.2	43 → 44	**202**
39	Davis Bay		11.6	0.7	1.7	27 → 36	**130**
40	Dumont d'Urville		8.2	0.5	1.2	35 → 42	**130**
41	Mertz Polynya		22.9	1.4	2.1	15 → 22	51
42	Ninnis Glacier		10.8	2.1	2.9	3 → 10	38
43	Wilson Hills		1.9	0.4	1.6	45 → 38	**344**
44	McMurdo Sound	Ross Sea	5.8	1.5	2.6	12 → 12	82
45	Terra Nova Bay		7.3	1.5	2.9	11 → 11	88
46	Ross Ice Shelf		239.6	1.8	2.1	8 → 21	17
	All polynyas		**646.9**	**1.8**	**2.2**		**23**
	All polynyas excl. the Ross Ice Shelf		**407.3**	**0.9**	**2.1**		**134**

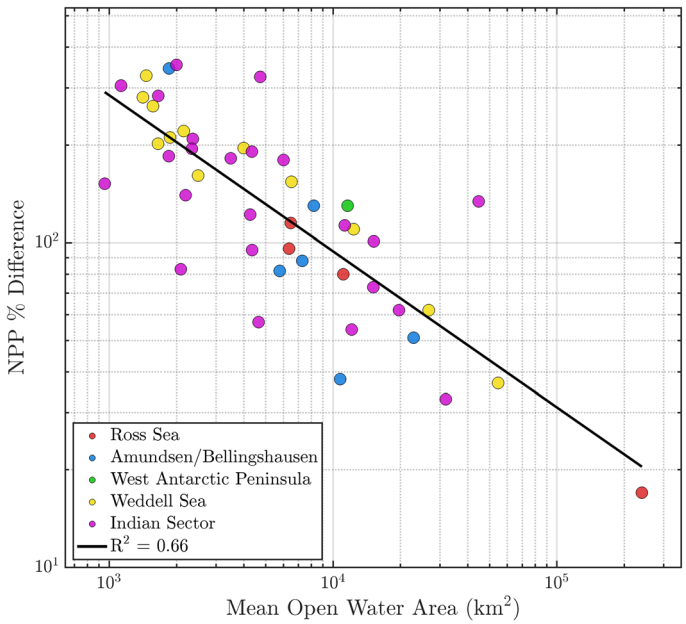

Fig. 5. Polynya NPP percentage difference from Table 1 plotted against the polynya mean 1998–2014 open water area reported in Arrigo et al. (2015), with a least-squares line derived in log–log-space, and colored by SOOS region. Note both axes are on a log scale.

shoreline (e.g., Krumhardt et al. 2024; St-Laurent et al. 2019) (Supporting Information Fig. S4). Accounting for adjacency can therefore explain some of the major spatial disparities between remote sensing–based NPP estimates and coupled physical–biogeochemical modeling–based NPP estimates by indicating that smaller polynyas represent more significant productivity hotspots than previously indicated by analyses of OBPG/L2gen Chl *a* products.

Given the substantial impacts adjacency can have on polynya productivity estimates, care should be taken when considering trends in coastal Antarctic productivity using many standard ocean color Chl *a* algorithms, especially for small polynyas. Potential future increases in open water area within small polynyas could lead to a spurious increase in remotely sensed polynya Chl *a* estimates if adjacency effects are not managed, potentially impacting analyses of drivers of polynya productivity and climate-level trends.

While the unique optical properties of Antarctic coastal waters have been known to differ from the average global relations used to fit the reflectance-based Chl *a* algorithms (e.g., Greg Mitchell and Holm-Hansen 1991; Pereira and Garcia 2018; Reynolds et al. 2001; Robinson et al. 2021), these results further illustrate that using atmospheric correction methods sensitive to adjacency effects are also likely to impair our

ecological understanding of rapidly changing Antarctic polynyas. While POLYMER shows improved performance near ice, it is also constrained by a bio-optical water reflectance model that may not be well-adapted for the Antarctic. Further research is also needed to explore how in-water properties such as pigment packaging, relatively low backscattering, and relatively low content of dissolved substances may also contribute to underestimation of Chl *a* by ocean color satellites in coastal Antarctica. Regardless, Chl *a* is just one metric of ocean biology and productivity. Gaining a better understanding of the role of phytoplankton community composition and bio-optical properties of the phytoplankton and water column will be important to better model pigments, NPP, and carbon uptake.

Author Contributions

Conceptualization: Hilde Oliver, Jessica S. Turner, and Heidi Dierssen. Methodology: Hilde Oliver, Jessica S. Turner, Alexandre Castagna, Henry Houskeeper, and Heidi Dierssen. Satellite product analysis: Hilde Oliver. Radiative transfer modeling: Alexandre Castagna. Writing (1st draft): Hilde Oliver. Editing (2nd-nth draft): Hilde Oliver, Jessica S. Turner, Alexandre Castagna, Henry Houskeeper, and Heidi Dierssen.

Acknowledgments

Hilde Oliver and Henry Houskeeper were supported by the WHOI Innovation month, and Hilde Oliver was also supported by NSFGEO-NERC project 1941483. Jessica Turner and Heidi Dierssen acknowledge funding from NASA Ocean Biology and Biogeochemistry (80NSSC20K1518 and 80NSSC24K0481). Alexandre Castagna was supported by the RAdCor project (BELSPO contract SR/00/406). We gratefully acknowledge Gert van Dijken and Kevin Arrigo for providing the polynya masks. We acknowledge the support from ASLO and Wiley in the form of an APC waiver offered to Hilde Oliver via the *L&O Letters* Early Career Publication Honor. We acknowledge NASA OB.DAAC and the use of OC-CCI data.

References

Arrigo, K. R. 2015. *Discrete fluorometric Chlorophyll-a Data From RVIB Nathaniel B* Palmer NBP1005 in the Amundsen Sea, Southern Ocean 73 S 115 W from 2010–2011 (ASPIRE project) (Version 29 January 2015) [Data set]. Biological and Chemical Oceanography Data Management Office (BCO-DMO). https://www.bco-dmo.org/dataset/546372.

Arrigo, K. R., K. E. Lowry, and G. L. van Dijken. 2012. "Annual Changes in Sea Ice and Phytoplankton in Polynyas of the Amundsen Sea, Antarctica." *Deep-Sea Research Part II: Topical Studies in Oceanography* 71–76: 5–15. https://doi.org/10.1016/j.dsr2.2012.03.006.

Arrigo, K. R., G. L. Van Dijken, and A. L. Strong. 2015. "Environmental Controls of Marine Productivity Hot Spots around Antarctica." *Journal of Geophysical Research: Oceans* 120, no. 8: 5545–5565. https://doi.org/10.1002/2015JC010888.

Arrigo, K. R., G. L. van Dijken, and S. Bushinsky. 2008*b*. "Primary Production in the Southern Ocean, 1997–2006." *Journal of Geophysical Research: Oceans* 113, no. 8: 1997–2006. https://doi.org/10.1029/2007JC004551.

Arrigo, K. R., G. L. van Dijken, and S. Pabi. 2008*a*. "Impact of a Shrinking Arctic Ice Cover on Marine Primary Production." *Geophysical Research Letters* 35, no. 19: 1–6. https://doi.org/10.1029/2008GL035028.

Bailey, S. W., B. A. Franz, and P. J. Werdell. 2010. "Estimation of near-Infrared Water-Leaving Reflectance for Satellite Ocean Color Data Processing." *Optics Express* 18, no. 7: 7521–7527. https://doi.org/10.1364/OE.18.007521.

Bélanger, S., J. K. Ehn, and M. Babin. 2007. "Impact of Sea Ice on the Retrieval of Water-Leaving Reflectance, Chlorophyll a Concentration and Inherent Optical Properties from Satellite Ocean Color Data." *Remote Sensing of Environment* 111, no. 1: 51–68. https://doi.org/10.1016/j.rse.2007.03.013.

Bulgarelli, B., V. Kiselev, and G. Zibordi. 2014. "Simulation and Analysis of Adjacency Effects in Coastal Waters: A Case Study." *Applied Optics* 53, no. 8: 1523–1545. https://doi.org/10.1364/AO.53.001523.

Castagna, A., and Q. Vanhellemont. 2025. "A Generalized Physics-Based Correction for Adjacency Effects." *Applied Optics* 64, no. 10: 2719–2743. https://doi.org/10.1364/AO.546766.

Dierssen, H. M., and R. C. Smith. 2000. "Bio-Optical Properties and Remote Sensing Ocean Color Algorithms for Antarctic Peninsula Waters." *Journal of Geophysical Research* 105, no. C11: 26301–26312. https://doi.org/10.1029/1999JC000296.

Dierssen, H. M., M. Vernet, and R. C. Smith. 2000. "Optimizing Models for Remotely Estimating Primary Production in Antarctic Coastal Waters." *Antarctic Science* 12, no. 1: 20–32. https://doi.org/10.1017/S0954102000000043.

Ferreira, A., A. C. Brito, C. R. B. Mendes, et al. 2022. "OC4-SO: A New Chlorophyll-a Algorithm for the Western Antarctic Peninsula Using Multi-Sensor Satellite Data." *Remote Sensing* 14, no. 5: 1052. https://doi.org/10.3390/rs14051052.

Frouin, R., P.-Y. Deschamps, D. Ramon, and F. Steinmetz. 2012. "Improved Ocean-Color Remote Sensing in the Arctic Using the POLYMER Algorithm." In *Proceedings of the SPIE Asia-Pacific Remote Sensing*, edited by R. J. Frouin, N. Ebuchi, D. Pan, and T. Saino, 85250I. Kyoto, Japan: SPIE. https://doi.org/10.1117/12.981224.

Gordon, H. R., and M. Wang. 1994. "Retrieval of Water-Leaving Radiance and Aerosol Optical Thickness Over the Oceans with SeaWiFS: A Preliminary Algorithm." *Applied*

Optics 33, no. 3: 443–452. https://doi.org/10.1364/AO.33.000443.

Hu, C., L. Feng, Z. Lee, et al. 2019. "Improving Satellite Global Chlorophyll a Data Products Through Algorithm Refinement and Data Recovery." *Journal of Geophysical Research: Oceans* 124, no. 3: 1524–1543. https://doi.org/10.1029/2019JC014941.

Ibrahim, A., B. A. Franz, Z. Ahmad, and S. W. Bailey. 2019. "Multiband Atmospheric Correction Algorithm for Ocean Color Retrievals." *Frontiers in Earth Science* 7. https://doi.org/10.3389/feart.2019.00116.

IOCCG. 2015. "Ocean Colour Remote Sensing in Polar Seas." In *Reports and Monographs of the International Ocean Colour Coordinating Group*. IOCCG Report Series No. 16, edited by M. Babin, K. Arrigo, S. Bélanger, and M.-H. Forget. Dartmouth, Canada: International Ocean Colour Coordinating Group.

Jackson, T., S. Sathyendranath, and F. Mélin. 2017. "An Improved Optical Classification Scheme for the Ocean Colour Essential Climate Variable and Its Applications." *Remote Sensing of Environment* 203: 152–161. https://doi.org/10.1016/j.rse.2017.03.036.

König, M., M. Hieronymi, and N. Oppelt. 2019. "Application of Sentinel-2 MSI in Arctic Research: Evaluating the Performance of Atmospheric Correction Approaches Over Arctic Sea Ice." *Frontiers in Earth Science* 7. https://doi.org/10.3389/feart.2019.00022.

Krumhardt, K. M., M. C. Long, C. M. Petrik, et al. 2024. "From Nutrients to Fish: Impacts of Mesoscale Processes in a Global CESM-FEISTY Eddying Ocean Model Framework." *Progress in Oceanography* 227: 103314. https://doi.org/10.1016/j.pocean.2024.103314.

Labrousse, S., A. D. Fraser, M. Sumner, et al. 2019. "Dynamic Fine-Scale Sea Icescape Shapes Adult Emperor Penguin Foraging Habitat in East Antarctica." *Geophysical Research Letters* 46, no. 20: 11206–11218. https://doi.org/10.1029/2019GL084347.

Lee, Y. 2023*a*. *Chlorophyll-a concentration from the Amundsen Sea, Antarctica, 2061* [Data set]. Antarctica: KOPRI. https://doi.org/10.22663/KOPRI-KPDC-00000649.2.

Lee, Y. 2023*b*. *Chlorophyll-a concentration from the Amundsen Sea, Antarctica, 2018* [Data set]. Antarctica: KOPRI. https://doi.org/10.22663/KOPRI-KPDC-00001049.2.

Lee, Y. 2023*c*. *Chlorophyll-a concentration from the Amundsen Sea, Antarctica, 2020* [Data set]. Antarctica: KOPRI. https://doi.org/10.22663/KOPRI-KPDC-00001563.2.

Letelier, R. M., and M. R. Abbott. 1996. "An Analysis of Chlorophyll Fluorescence Algorithms for the Moderate Resolution Imaging Spectrometer (MODIS)." *Remote Sensing of Environment* 58, no. 2: 215–223. https://doi.org/10.1016/S0034-4257(96)00073-9.

Mitchell, G. B., and O. Holm-Hansen. 1991. "Bio-Optical Properties of Antarctic Peninsula Waters: Differentiation from Temperate Ocean Models." *Deep-Sea Research Part A, Oceanographic Research Papers* 38, no. 8: 1009–1028. https://doi.org/10.1016/0198-0149(91)90094-V.

Mobley, C. D., J. Werdell, B. Franz, Z. Ahmad, and S. Bailey. 2016. *Atmospheric Correction for Satellite Ocean Color Radiometry (No. GSFC-E-DAA-TN35509)*. NASA. https://oceancolor.gsfc.nasa.gov/resources/docs/technical/NASA-TM-2016-217551.pdf.

Ocean Colour Climate Change Initiative (OC-CCI). 2022. *Product User Guide for v6.0 Dataset (No. 6.1)*. Plymouth, UK: Plymouth Marine Laboratory (PML).

Palmer Station Antarctica LTER, and N. Waite. 2022. *Merged Discrete Water-Column Data From PAL LTER Research Cruises Along the Western Antarctic Peninsula, From 1991 to 2020*. Environmental Data Initiative. https://doi.org/10.6073/PASTA/65C43A4688ECCF8CA7CC3A2D07A0CC78.

Pereira, E. S., and C. A. E. Garcia. 2018. "Evaluation of Satellite-Derived MODIS Chlorophyll Algorithms in the Northern Antarctic Peninsula." *Deep Sea Research Part II: Topical Studies in Oceanography* 149: 124–137. https://doi.org/10.1016/j.dsr2.2017.12.018.

Reynolds, R. A., A. Matsuoka, T. Hirawake, S. Bélanger, and B. G. Mitchell. 2015. "Chapter 4: Ocean Colour Algorithms and Bio-Optical Relationships for Polar Seas." In *Ocean Colour Remote Sensing in Polar Seas*. USA: International Ocean Colour Coordinating Group (IOCCG).

Reynolds, R. A., D. Stramski, and B. G. Mitchell. 2001. "A Chlorophyll-Dependent Semianalytical Reflectance Model Derived From Field Measurements of Absorption and Backscattering Coefficients Within the Southern Ocean." *Journal of Geophysical Research: Oceans* 106, no. C4: 7125–7138. https://doi.org/10.1029/1999JC000311.

Robinson, C. M., Y. Huot, N. Schuback, T. J. Ryan-Keogh, S. J. Thomalla, and D. Antoine. 2021. "High Latitude Southern Ocean Phytoplankton Have Distinctive Bio-Optical Properties." *Optics Express* 29, no. 14: 21084–21112. https://doi.org/10.1364/OE.426737.

Smith, W. O., and D. E. Kaufman. 2018. "Climatological Temporal and Spatial Distributions of Nutrients and Particulate Matter in the Ross Sea." *Progress in Oceanography* 168(October): 182–195. https://doi.org/10.1016/j.pocean.2018.10.003.

Soppa, M. A., B. Silva, F. Steinmetz, et al. 2021. "Assessment of Polymer Atmospheric Correction Algorithm for Hyperspectral Remote Sensing Imagery Over Coastal Waters." *Sensors* 21, no. 12: 4125. https://doi.org/10.3390/s21124125.

St-Laurent, P., P. L. Yager, R. M. Sherrell, H. Oliver, M. S. Dinniman, and S. E. Stammerjohn. 2019. "Modeling the Seasonal Cycle of Iron and Carbon Fluxes in the Amundsen Sea Polynya, Antarctica." *Journal of Geophysical Research:*

Oceans 124, no. 3: 1544–1565. https://doi.org/10.1029/2018JC014773.

Steinmetz, F., P.-Y. Deschamps, and D. Ramon. 2011. "Atmospheric Correction in Presence of Sun Glint: Application to MERIS." *Optics Express* 19, no. 10: 9783. https://doi.org/10.1364/OE.19.009783.

Tanre, D., M. Herman, and P. Y. Deschamps. 1981. "Influence of the Background Contribution upon Space Measurements of Ground Reflectance." *Applied Optics* 20, no. 20: 3676–3684. https://doi.org/10.1364/AO.20.003676.

Tanre, D., M. Herman, P. Y. Deschamps, and A. De Leffe. 1979. "Atmospheric Modeling for Space Measurements of Ground Reflectances, Including Bidirectional Properties." *Applied Optics* 18, no. 21: 3587–3594. https://doi.org/10.1364/AO.18.003587.

Warren, S. G. 2013. "Can Black Carbon in Snow be Detected by Remote Sensing?" *Journal of Geophysical Research: Atmospheres* 118, no. 2: 779–786. https://doi.org/10.1029/2012JD018476.

Yager, P., R. Sherrell, S. Stammerjohn, et al. 2012. "ASPIRE: The Amundsen Sea Polynya International Research Expedition." *Oceanography* 25, no. 3: 40–53. https://doi.org/10.5670/oceanog.2012.73.

Yang, E. J. 2023. *Chlorophyll-a concentration from the Antarctic Amundsen Sea, 2014* [Data set]. Antarctica: KOPRI. https://doi.org/10.22663/KOPRI-KPDC-00000483.3.

Zeng, C., H. Xu, and A. Fischer. 2016. "Chlorophyll-a Estimation Around the Antarctica Peninsula Using Satellite Algorithms: Hints from Field Water Leaving Reflectance." *Sensors* 16, no. 12: 2075. https://doi.org/10.3390/s16122075.

Supporting Information

Additional Supporting Information may be found in the online version of this article.

Submitted 14 November 2024
Revised 13 May 2025
Accepted 08 June 2025